Journal of Statistical Physics, Vol. 93, Nos. 3/4, 1998

Ostwald Ripening in Two Dimensions: Treatment with Pairwise Interactions

Boris Levitan[1] and Eytan Domany[1]

Received February 10, 1998

Ostwald ripening is the last stage of the evolution of a system with two coexisting phases. It is a relatively simple nonequilibrium phenomenon with several interesting features. For example, as the system coarsens it goes through a scaling state, one which looks the same (up to an overall length scale, which grows) at all times. The dynamics of the problem can be mapped, in two dimensions, onto an evolving Coulomb system. In this work we present a brief summary of a novel theoretical approach to this problem, based on an analytic derivation (using a mean-field approach) of an effective two-body interaction between droplets of the minority phase. The resulting interacting many-body dynamics is solved by a very efficient numerical algorithm, allowing us to follow the evolution of more than 10^6 droplets on a simple workstation. The results are in excellent agreement with recent experiments.

KEY WORDS: Ostwald ripening; scaling state.

Ostwald ripening[1] is a coarsening process, observed during the late stage of the evolution of a two-phase system (say, solid in liquid), in the course of which the droplets of the minority phase exchange material by means of diffusion. This process leads towards a scaling state in which the characteristic length scale grows with time according to the Lifshitz–Slyozov law[2] $\bar{R}(t) \sim t^{1/3}$. When rescaled by $\bar{R}(t)$, all statistical characteristics of the system (such as droplet size distribution, spatial correlations, etc.) are time-independent.

We dedicate this paper to Leo Kadanoff on the occasion of his 60th birthday, and wish him many more years of fun and joy doing physics.

[1] Department of Physics of Complex Systems, Weizmann Institute, Rehovot 76100, Israel; e-mail: levitan@bfr.co.il, fedomany@weizmann.weizmann.ac.il.

0022-4715/98/1100-0501$15.00/0

These characteristics were studied in a number of detailed numerical simulations. The Cahn–Hilliard equation,[3,4] solved in the entire system, provides the most basic model of Ostwald ripening. If the solid droplets are assumed to be uniform and only their boundaries are retained to describe the system, the problem becomes fine of solving the diffusion equation for the concentration field $c(\vec{r})$ between droplets, with Gibbs–Thomson boundary conditions:[5]

$$c|_{droplet}(t) = c_{eq}(R(t)) = c_\infty + \frac{\alpha}{R(t)} \tag{1}$$

The boundaries move in response to the incident flux;

$$\frac{dR}{dt} = -J_\perp \qquad \vec{J} = -\nabla c|_R \tag{2}$$

At long times a quasi-static approximation can be used and the diffusion problem turns into Poisson's equation in $2-d$,

$$\nabla^2 c = 0 \tag{3}$$

This problem can be reduced to an implicit system of ordinary differential equations.[6–8] Since these calculations take into account *all* the complicated interactions between the droplets, mediated by the diffusion field, they do not elucidate the relative importance of different aspects of these interactions. The number of droplets and the length of the simulations are also limited. On the other end of the complexity scale are analytical mean field treatments[2,9,10] that neglect *all* spatial effects; these, however, are too simple to account for correlations in a system of nonvanishing volume fraction. Previous attempts to "interpolate" between these extremes, and provide an analytical treatment of the spatial effects[11,12] contain uncontrolled approximations[13] and lead to very complicated expressions.

Using a mean-field type approximation, we calculated *analytically* pairwise interactions between the droplets. These appear in closed-form dynamic equations for many interacting droplets, which are integrated numerically. Our model gives rise to a very efficient numerical algorithm; the evolution of tens of thousands of droplets can be followed. Our work was motivated by and our results are compared with a recent experiment on a two-dimensional film of liquid and crystalline succinonitrile in coexistence.[14] This experiment shows that even at $\varphi = 0.4$ the droplets are almost circular; therefore we characterize the system by the set of the droplets' radii R_i and the positions $\vec{r}_i$ of their centers.

We write the solution of Eq. (3) in terms of "charges" and "dipoles" placed at $\vec{r}_i$

$$c(\vec{r}) = \sum_i q_i \log(|\vec{r} - \vec{r}_i|/R_0) + \sum_i \frac{(\vec{p}_i \cdot (\vec{r} - \vec{r}_i))}{|\vec{r} - \vec{r}_i|^2} \tag{4}$$

(R_0 is an arbitrary length). The boundary conditions (1) on the surface of each droplet give rise to linear equations which determine the charges q_i and the dipoles $\vec{p}_i$. When the resulting solution is used in (2) to derive the flux at droplet i, we find that it's normal component has two terms. One is isotropic, due to the charges; it affects the droplet's area and therefore determines the dynamics of the radii. The other is an anisotropic contribution, due to the dipoles, which gives rise to a shift of the centers of the droplets.[11, 15] The charges and dipoles can be eliminated, yielding[15] dynamic equations for the radii and positions of the droplets:

$$\dot{R}_i = \frac{q_i}{R_i} = \sum_j L^{-1}_{i,j}(1 + R_j/R_c) = \sum_j L^{-1}_{i,j} \tag{5}$$

$$\frac{d\vec{r}_i}{dt} = -\frac{2\vec{p}_i}{R_i^2} = 2 \sum_{j \neq i} R_j \dot{R}_j \frac{\vec{X}_{i,j}}{|X_{i,j}|^2} \tag{6}$$

where $X_{i,j} = |\vec{r}_j - \vec{r}_i|$ and $R_c = \alpha/c_\infty$ is a capillary length. For the first equality in (6) see ref. 11; the second is obtained from the anisotropic part of the boundary condition at the droplet's surface.[15] The second equality in Eq. (5) is due to a sum rule;[15, 16] $L^{-1}_{i,j}$ are the elements of the *inverse* of the matrix $\hat{L}$, defined as:[6]

$$L_{i,j} = R_i R_j \begin{cases} \log(R_i/R_0) & \text{if } i = j \\ \log(X_{i,j}/R_0) & \text{otherwise} \end{cases} \tag{7}$$

The value of the parameter R_0 is *arbitrary*; it does not affect the dynamics of the system.[15] Once $\hat{L}$ has been inverted, we can evaluate the radii at the next time step. One must invert the $N \times N$ matrix $L_{i,j}$ at *each* time step (which takes $O(N^3)$ operations); since we need $O(N)$ time steps, each run would cost $O(N^4)$ computations.

Beenakker[17] solved an analogous problem in $3 - d$ by *truncating* the matrix $L_{i,j}$. Motivated by the effect of *screening*,[18, 19] he took into account only interactions between those droplets whose separation does not exceed a threshold. Akaiwa and Meiron[8] used the analogous truncation procedure in $2 - d$. However, formal truncation of the matrix seems problematic. Since the matrix elements *grow* with $X_{i,j}$, the elements of the *inverse* matrix

$\hat{L}^{-1}$ as functions of the cutoff should contain large fast oscillating components. Apparently, the success of Akaiwa and Meiron[8] is due to the fact that these oscillations are effectively averaged out during the run.

Rather than discarding large matrix elements and proceeding to invert the truncated matrix numerically, we calculate analytically the elements of $\hat{L}^{-1}$, using a mean field approximation. First, represent $\hat{L}$ as the sum of its diagonal and off diagonal parts, $\hat{L} = \hat{L}_0 - \hat{L}_1$, where $(\hat{L}_0)_{i,j} = \delta_{i,j} R_i^2 \log(R_i/R_0)$ and $(\hat{L}_1)_{i,j} = -(1-\delta_{i,j}) R_i R_j \log(X_{i,j}/R_0)$ and introduce a new matrix $\hat{T}$ defined by

$$\hat{L}^{-1} = \hat{L}_0^{-1} + \hat{L}_0^{-1} \hat{T} \hat{L}_0^{-1}$$

This is indeed the inverse of $\hat{L}$ if $\hat{T}$ satisfies the equation

$$\hat{T} = \hat{L}_1 + \hat{L}_1 \hat{L}_0^{-1} \hat{T} \tag{8}$$

For convenience we represent $T_{i,j} = R_i R_j \phi_{i,j}$; Eq. (8) now becomes a condition on the matrix $\hat{\phi}$, which we write separately for the diagonal and off-diagonal elements:

$$\phi_{k,k} = -\sum_{j \neq k} \frac{\log(X_{k,j}/R_0)}{\log(R_j/R_0)} \phi_{j,k} \tag{9}$$

$$\sum_{j \neq i,k} \frac{\log(X_{i,j}/R_0)}{\log(R_j/R_0)} \phi_{j,k} + \phi_{i,k} = -\gamma_k \log(X_{i,k}/R_0) \tag{10}$$

with

$$\gamma_k = 1 + \frac{\phi_{k,k}}{\log(R_k/R_0)} \tag{11}$$

The set of Eqs. (9)–(11) is exact but solving it is as difficult as inverting $\hat{L}$. The advantage of this formalism is that it serves as a convenient starting point to generate *approximate* expressions for $\phi_{i,j}$—in particular, a manageable mean-field approximation.

We give now an outline of the main ideas and formal steps of the derivation of our approximation to $\phi_{i,j}$; details will be presented elsewhere.[15] First of all we assume that the i, j matrix element depends only on the corresponding distance,[20] $\phi_{i,j} = \phi(X_{i,j})$, and that $\phi(X)$ varies only on scales ζ such that the number of droplets within an area ζ^2 is large. If this holds we can replace in Eqs. (10) and (9) the factor $1/\log(R_j/R_0)$ by its mean value and the sums by integrals. Within this mean-field approximation Eq. (9) implies $\phi_{k,k}^{(mf)} = \text{const.} = \phi_0$; this leads to a self-consistent expression[15] for $\phi(X_{i,j})$ only if we set $\gamma_k = \text{const.} = \gamma_0$ which, in

turn, means (see Eq. (11)) that $\phi_0 = 0$ and $\gamma_0 = 1$. Thus within our mean-field treatment of $\hat{\phi}$, Eq. (10) becomes

$$\frac{1}{2\pi\zeta^2}\int \log\left(\frac{X_{i,j}}{R_0}\right)\phi(X_{j,k})\,d^2r_j - \phi(X_{i,k}) = \log\frac{X_{i,k}}{R_0} \tag{12}$$

where we introduced a constant length, defined by

$$\zeta^{-2} = 2\pi n\left\langle\frac{1}{\log(R_0/R)}\right\rangle \approx 2\pi n\frac{1}{\log(R_0/\langle R\rangle)} \tag{13}$$

Here $n = \varphi/\pi\langle R^2\rangle$ is the number of droplets per unit area; the angular brackets denote averaging over the droplet size distribution. Operating with ∇_i^2 on Eq. (12) yields the differential equation

$$-\zeta^{-2}\phi + \nabla^2\phi = -2\pi\,\delta(\vec{r}) \tag{14}$$

which is solved by the zeroth order modified Bessel function of the second kind (also called Mac-Donald function), $\phi(X) = K_0(X/\zeta)$. This determines the *off-diagonal* elements of $\phi_{i,j}$ up to the length ζ which depends on the arbitrary parameter R_0. Since the value of this parameter does not affect the *exact* solution of the problem, we can tune it to improve our approximation. Note that when our $\phi(X)$ is used in the integral form of Eq. (9) we get

$$\frac{1}{2\pi\zeta^2}\int \log(X_{k,j}/R_0)\,K_0(X_{j,k}/\zeta)\,d^2r_j = \phi_{k,k} = \phi_0 = 0 \tag{15}$$

After some lengthy algebra, presented elsewhere,[15] we can show that this condition is satisfied when R_0 satisfies the following *approximate* expression:

$$\left\langle\frac{1}{\log(R_0/R)}\right\rangle \approx \left\langle\frac{1}{K_0(R/\zeta)}\right\rangle \tag{16}$$

By substituting Eq. (16) in Eq. (13) we eliminate R_0 from the problem and obtain an equation for ζ:

$$\zeta^{-2} = 2\pi n\left\langle\frac{1}{K_0(R/\zeta)}\right\rangle \tag{17}$$

which is almost identical to Marqusee's expression for the screening length.[10] The solution for $\phi(X)$ determines the matrix $\hat{T}$ and we get an

expression for the matrix elements $L^{-1}_{i,j}$ which, when used in Eq. (5) together with the relation[15]

$$-\sum_{j\neq i}\frac{1}{\log(R_j/R_0)}K_0\left(\frac{X_{i,j}}{\zeta}\right)\approx\frac{1}{2\pi\zeta^2}\int K_0\left(\frac{r}{\zeta}\right)d^2r=1$$

finally yields our central result:

$$R_i\frac{dR_i}{dt}=R_i\sum_j L^{-1}_{i,j}=\frac{1}{K_0(R_i/\zeta)}\sum_{j(\neq i)}\frac{K_0(X_{i,j}/\zeta)}{K_0(R_j/\zeta)}\left(\frac{1}{R_j}-\frac{1}{R_i}\right) \tag{18}$$

Since $K_0(x)\sim\exp(-x)$ for large x, ζ indeed has the meaning of a screening length. Note that the total area of the droplets is conserved by Eq. (18).

The approximations made, of replacing the sums by integrals and $1/\log(R_j/R_0)$ by its average value $1/(2\pi\zeta^2)$, are valid if the function $\phi(X)$ is smooth and the number of droplets in the screening zone is large: $N_\zeta=n\zeta^2\gg 1$. For $\varphi=0.13$ (as used in the experiment) the approach outlined above gave a much too small value for ζ. A somewhat larger value was obtained[15] by taking into account the fact that each of the droplets is surrounded by a *depletion zone*, from which all neighbors are excluded. Including depletion zones retains an equation of the same form as Eq. (18) for the evolution of the radii, but with the mean-field ζ replaced by $\zeta_{sc}>\zeta$. For $\varphi=0.13$ it becomes $\zeta_{sc}=2.73\bar{R}\approx 0.56X$ where X is the typical distance between neighbors. This value is obtained from solving a set of equations which, in the low concentration limit, approach Eq. (17). Although ζ_{sc} is still too small to provide a formal support to our approach, we tested it by integrating (numerically) Eqs. (18) and (6).

The detailed description of our numerical algorithm is presented elsewhere.[15] An advantage of our method is that it conserves the total area of the droplets at each time step. Computational efficiency is very high: an entire run, starting with N droplets initially and running till most disappear (i.e., reach $R_i\approx 0$) takes only $O(N\log N)$ operations. This is due to the fact that we are able to keep the time step reasonably large, eliminating a large number of droplets at each step. At the same time, unlike previous studies,[8, 17, 21] we ensure *exact* conservation of the total area of the droplets at each time step. This makes our approach useful for an extensive study of the Ostwald problem.

We used initial systems of up to $1.2\cdot 10^6$ droplets with toroidal boundary conditions. First evaluate $\dot{R}_i$ using Eq. (18) with $\zeta=2.73\bar{R}$; next use Eq. (6) to calculate the motion of the droplets' centers.

Regarding this motion, one can use Eq. (6) to estimate its importance[11, 15] by comparing the characteristic times for significant shift versus

a shrinking droplet's lifetime; $\tau_{\text{shift}}/\tau_{\text{life}} \sim (X^2/R^2) \approx \pi/\varphi$. Hence for small fractions (and even for $\varphi = 0.13$) the shift of the droplets is *adiabatically* slower than the droplets' growth and one is tempted to neglect the motion of the centers. Indeed we tried this, but the resulting solution of the dynamics of the radii alone led to severe inconsistencies (manifest in significant overlap of neighboring droplets, i.e., $R_i + R_j > X_{i,j}$). This convinced us that the correlations induced by the proper movement of the droplets are essential for a physically sensible solution.

The sum on the r.h.s. of Eq. (6) appears to have convergence problems; assuming that the charges q_j are uncorrelated random variables, with zero mean (as required by the total area conservation) one can easily get

$$\left\langle \left(\frac{d\vec{r}_i}{dt} \right)^2 \right\rangle \sim \langle q^2 \rangle \sum \frac{1}{|X_{i,j}|^2} \sim \langle q^2 \rangle \log L_s \tag{19}$$

where L_s is the size of the system. The charges, however, *are* correlated (the effect of screening) and this causes fast convergence.[15] We performed in some cases the entire sum and then repeated the simulations, summing only over droplets j with $|X_{i,j}| < b$, using $b = 2.3X$ and $b = 3.25X$ (the latter value corresponds to about 10 terms in the sum); no significant difference between these three simulations was found.

First we tried to evaluate the distribution of the droplets' radii in the scaling state (see Fig. 1). Our previous studies[15] yielded only limited agreement with the experimentally obtained distribution and, since this function has been measured with considerable precision, we decided to integrate the evolution of a very large system, to check whether the observed deviations are due to the fact that with smaller systems we did not reach the asymptotic scaling regime.

For 1,200,000 initial droplets at $\varphi = 0.13$ we started taking data when the number of droplets was 30,000; beyond this point the size distribution did not change noticeably, indicating that we have reached the scaling regime. The agreement with the measurements of Krichevsky and Stavans is very good.

The system approached the scaling state at $N \approx 3000$; this is when we started our measurements. In order to reduce fluctuations we averaged all the data over 8 runs. Such a run took about 30 hours on a single processor of an HP-9000 (series K200) workstation. First we present the distribution of the droplets' radii in the scaling state (see Fig. 1). The agreement with the experimental points[14] is reasonable. It is interesting to note that our distribution agrees very well with that of Akaiwa and Meiron (see Fig. 20 of ref. 8).

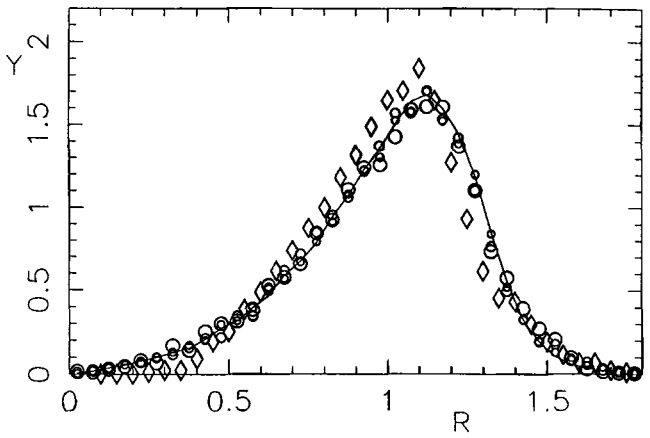

Fig. 1. The size distribution of the droplets; R is normalized by $\bar{R}$. Data were taken when the number of droplets (initially 1,200,000) decreased to $N = 30{,}000$ (*largest circles*), $N = 15,000$ (*medium circles*) and $N = 7000$ (*small circles*). Each plot presents the average over 8 runs; the solid line is a guide to the eye. The fact that at these times the same distribution was obtained indicates that we reached the scaling state. The experimental result of Krichevsky and Stavans is also shown (*diamonds*).

A much more demanding comparison is that of various correlation functions that were also measured by Krichevsky and Stavans. Figure 2 presents the correlation function $G(r)$—the probability to find a droplet's center at a distance r from a given droplet's center, as obtained by our numerical solution and experiment. To get these data we run systems with

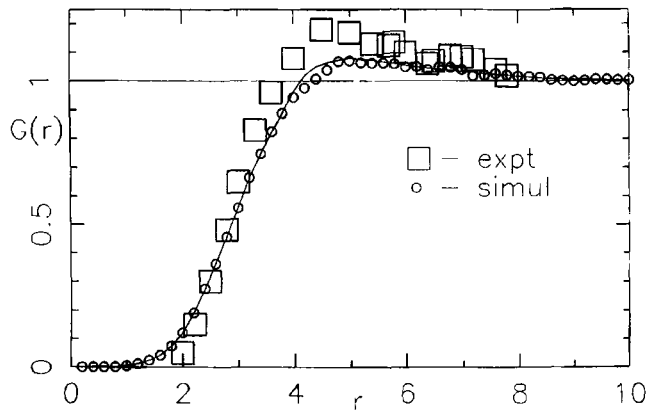

Fig. 2. Weighted time average of the correlation functions of droplets' positions, $G(r)$, taken at different times in the scaling state, each averaged over 8 runs (*circles*); the experimental results of Krichevsky and Stavans (*squares*). The solid line is a guide to the eye.

50,000 initial droplets; at $\varphi = 0.13$ the system appeared to approach the scaling state at $N \approx 3000$, at which point we started our measurements. In order to reduce fluctuations we averaged all the data over 8 runs. We recovered the position of the initial rise of $G(r)$ as well as the existence and position of its maximum. The value of our curve at the maximum is smaller than the experimental one; our $G(r)$ is rather close to the result of Masbaum, obtained by solving the Cahn-Hilliard equation (see Fig. 1a in ref. 4), that also exhibits a small peak. Akaiwa and Meiron,[8] on the other hand, obtain with their dipole approximation a peak which slightly overshoots and then decreases below the experimental points.

We measured also the correlation functions of the *charges*, defined first in ref. 14, which contain more detailed information about the system. For a charge q_i calculate $Q_+(r)$, the total amount of similar charge within an annulus $[r, r+dr]$ around $\vec{r}_i$ and define the function

$$g_+(r) = \langle q_i Q_+(r) \rangle$$

Similarly we define $g_-(r)$ in terms of the *opposite* charges. These two functions, as obtained by our simulations, are presented in Fig. 3 together with the corresponding experimental data of Krichevsky and Stavans. We find the agreement between theory and experiment quite impressive.

In summary, we introduced and tested a model for the Ostwald ripening process in two dimensions. Our model approximates the exchange of material between the droplets, as determined by the complicated diffusive interaction, by simple pairwise couplings. An approximate mean field

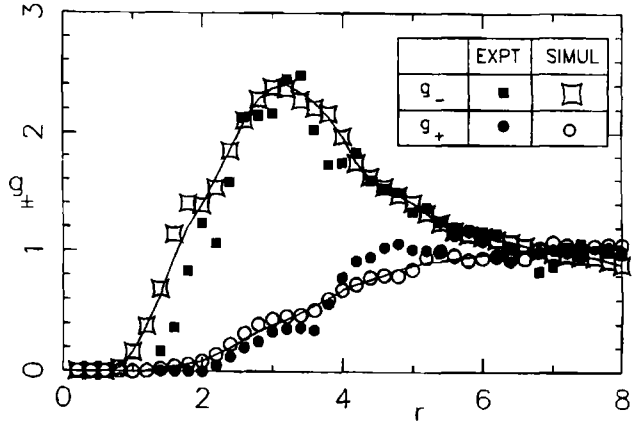

Fig. 3. The correlation functions for the same and opposite charges, as obtained by our simulations and by experiments. Our data present averages over 8 runs. The solid line is a guide to the eye.

type approach is used to evaluate these pairwise interactions. The resulting dynamic equations are then solved numerically. Our model gives good agreement with experiment for a fairly large value of area fraction. We found that the shift of the droplets plays an important role at $\varphi = 0.13$. Our method leads to a very efficient numerical algorithm that can be useful for future studies of this problem.

ACKNOWLEDGMENTS

This research was supported by grants from the Germany-Israel Science Foundation (GIF). B. L. thanks the Clore Foundation for financial support. We thank O. Krichevsky, J. Stavans and D. Kandel for discussions.

REFERENCES

1. W. Ostwald, *Z. Phys. Chem.* **34**:495 (1900).
2. E. M. Lifshitz and V. V. Slyozov, *J. Phys. Chem. Solids* **19**:35 (1961); E. M. Lifshitz and L. P. Pitaevskii, *Physical Kinetics* (Pergamon Press Oxford, 1982), Vol. 432.
3. T. M. Rogers and R. C. Desai, *Phys. Rev. B* **39**:11956 (1989).
4. N. Masbaum, *J. Phys. I France* **5**:1143 (1995).
5. $R(t)$ is the local radius of curvature.
6. T. Imaeda and K. Kawasaki, *Physica A* **164**:335 (1990).
7. N. Akaiwa and P. W. Voorhees, *Phys. Rev. E* **49**:3860 (1994).
8. N. Akaiwa and D. I. Meiron, *Phys. Rev. E* **51**:5408 (1995).
9. C. Wagner, *Z. Electrochem.* **65**:581 (1961).
10. J. A. Marqusee, *J. Chem. Phys.* **81**:976 (1984).
11. M. Marder, *Phys. Rev. A* **36**:858 (1987).
12. Q. Zheng and J. D. Gunton, *Phys. Rev. A* **39**:4848 (1989).
13. As we show below, our treatment also has an uncontrolled approximate aspect in that the small parameter we identify is not really small at the experimentally relevant area fraction of 0.13.
14. O. Krichevsky and J. Stavans, *Phys. Rev. Lett.* **70**:1473 (1993); *Phys. Rev. E* **52**:1818 (1995).
15. B. Levitan and E. Domany, *Phys. Rev. E.* **57**:1895 (1998).
16. C. W. J. Beenakker and J. Ross, *J. Chem. Phys.* **83**:4710 (1985).
17. C. W. J. Beenakker, *Phys. Rev. A* **33**:4482 (1986).
18. M. Marder, *Phys. Rev. Lett.* **55**:2953 (1985).
19. J. A. Marqusee and J. Ross, *J. Chem. Phys.* **80**:536 (1984).
20. In general the diffusion field induces "many-body" interactions between droplets. Our assumption amounts to keeping pairwise interactions only.
21. J. H. Yao, K. R. Elder, H. Guo, and M. Grant, *Phys. Rev. B* **47**:14, 110 (1993).